




# Liquid jet stability through elastic planar nozzles

Md Emazuddin Alif<sup>1</sup>, Julie Veihdeffer<sup>1</sup>, Md Erfanul Alam<sup>2</sup>, and Andrew K. Dickerson<sup>1,a</sup> 

<sup>1</sup> Mechanical, Aerospace, and Biomedical Engineering, University of Tennessee, Knoxville, USA

<sup>2</sup> Mechanical Engineering, North Central College, Naperville, IL, USA

Received 20 June 2022 / Accepted 9 August 2022 / Published online 14 September 2022

© The Author(s), under exclusive licence to EDP Sciences, Springer-Verlag GmbH Germany, part of Springer Nature 2022

**Abstract** An extensive number of processes require liquid jets such as cleaning, waterjet cutting, hydroentanglement, and atomization in combustion. The coherence and stability of the jet highly depend on the characteristics of the nozzle. Jet breakup lengths have been extensively studied for a multitude of nozzle characteristics and external stimuli, yet jets issuing from deformable, elastic nozzles have not been considered. In this study, we take the enduring topic of jet breakup into a new realm by introducing nozzles that passively deform when exposed to liquid flow by making an approximately 500  $\mu\text{m}$  orifice in thin sheets. We perform the experiments with nozzles of varying hardness and thickness, starting with a rigid BeCu nozzle, and continuing with shore hardness 70A, 65A, 35A and 20A. We observe nozzle dilation scales well with Reynolds number and that softer nozzles experiences greater dilation, as expected. We introduce a modification to linear stability theory to describe the break-up length of deformable nozzles to account for the dilation, a scaling which works best for our stiffer nozzles. The three softest materials provide the most stable jets through the range of flow rates in which they can operate before failure. For all nozzles, breakup is highly variable with time and jet velocity.

**Keywords** Deformable membrane · Atomization · Linear stability · Nozzle dilation

## 1 Introduction

Liquid jet stability has captivated fluid mechanicians for nearly two centuries [1, 2], owing to both their mathematical complexity [3–9] and usefulness [10–12], and are of interest to the engineering and medical communities for their use in drug delivery [13, 14], inkjet printers [15], micro-fabrication [16, 17], cleaning of foulants [18, 19], and chemical synthesis [20]. It is critical to control the breakup distance and directionality of these jets so the drops they produce find the intended location and distance. Current methods for control include capillary breakup [21], breakup induced by a co-flowing gas [22, 23], passive inlet conditions and nozzle geometry [24–28], and active external forcing [29, 30]. In this experimental study, we present another passive means to modulate jet stability, elasticity in the nozzle. In such nozzles, liquid and solid dynamics are coupled. The deforming nozzle transforms jet velocity and breakup across a range of flow rates.

Liquid forced through a nozzle eventually breaks into a string of droplets. The length of a coherent liquid column is governed by several factors including surface tension, jet velocity, ambient pressure, viscosity of the liquid, and turbulence of the nozzle, but this is not a comprehensive list [5, 6, 31, 32]. Liquid jets may be classified into one of four breakup regimes [5, 6, 31, 32] based on their liquid and gas Weber numbers  $We = \rho V_0^2 D / \sigma$  and  $We_G = \rho_G V_0^2 D / \sigma$ , respectively, where  $\rho = 1 \text{ g/cm}^3$  and  $\rho_G = 0.0012 \text{ g/cm}^3$  are liquid and air densities,  $V_0$  is the jet exit velocity,  $D$  is the diameter of a circular nozzle, and  $\sigma$  is the liquid surface tension. Here we are concerned with the first two, the Rayleigh and first wind-induced breakup regimes. The Rayleigh regime begins following the transition from dripping to jetting, jets with  $We > 8$  and  $We_G < 0.4$  breakup due to capillary pinching. Gas inertia becomes important in the first wind-induced breakup regime [33] for  $0.4 < We_G < 13$ , where a jet from a traditionally rigid nozzles reaches its maximum length [34, 35]. At greater  $We$ , jets enter the second wind-induced breakup regime where jets are broken by dynamic gas pressure and damped by surface tension [34]. In the second wind-induced regime, increasing  $We$  decreases breakup length. A further increase in  $We$  pushes jets into the atomization regime where the jet is disintegrated at the nozzle exit.

Numerous theoretical and experimental investigations have been carried out to explain the disintegration of liquid jets [5]. Various forces act on the surface of

<sup>a</sup> e-mail: [ad@utk.edu](mailto:ad@utk.edu) (corresponding author)

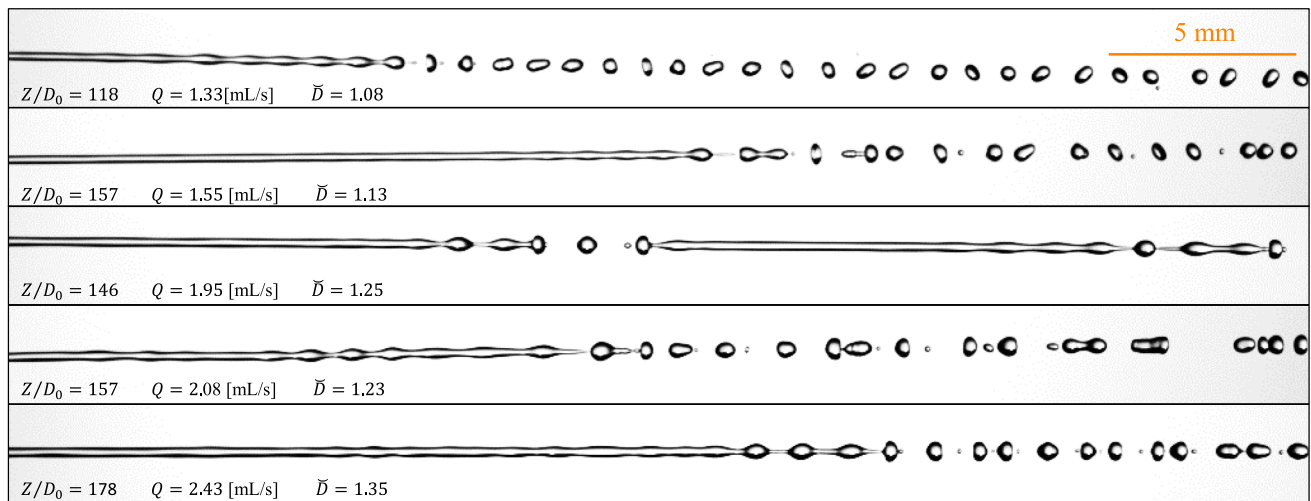


**Fig. 1** Photographic depictions of jet breakup for membrane 35A [ $Eh = 0.77$  (kN/m)] for increasing flow rates, top to bottom. Jets exhibit highly variant breakup lengths

jets leading to disturbances which are amplified when carried downstream, ultimately leading to jet breakup [5, 36]. Rayleigh (1878, 1879) was the first to derive a relation of the disturbance growth rate for inviscid jets emitted into a vacuum [21, 37]. Weber (1931) improved Rayleigh's one-dimensional model by incorporating liquid and gas viscosity [38]. Others have followed to further improve our understanding [30, 35, 39–46]. The majority of free jet studies derive modeling from linear temporal stability analysis such that axisymmetric disturbances grow exponentially in time until the amplitude of disturbances grows larger than the jet radius, signaling breakup. It is unclear if any of the aforementioned theoretical approaches are appropriate for jets in which the nozzle participates in initial disturbance production/absorption and reacts to changes in flow.

In this study, we measure the breakup and nozzle dilation characteristics for jets issuing from a nearly planar, elastic membrane. In this case, we refer to elastic as those materials which notably deform at our relatively low velocities (1.72–19.12 m/s). Nozzles begin approximately as 500- $\mu\text{m}$  diameter circles but can produce jets > 1250  $\mu\text{m}$  in diameter in some cases. Nozzle dilation under increasing flow rates, elastic effects, and the crude geometry of our nozzles creates jets with a large variance in breakup length, as shown in Fig. 1. We present our experimental methods in Sect. 2. Jet breakup metrics and nozzle behavior is presented in Sects. 3–5. We discuss the implications of our work and conclude in Sect. 6.

## 2 Methods

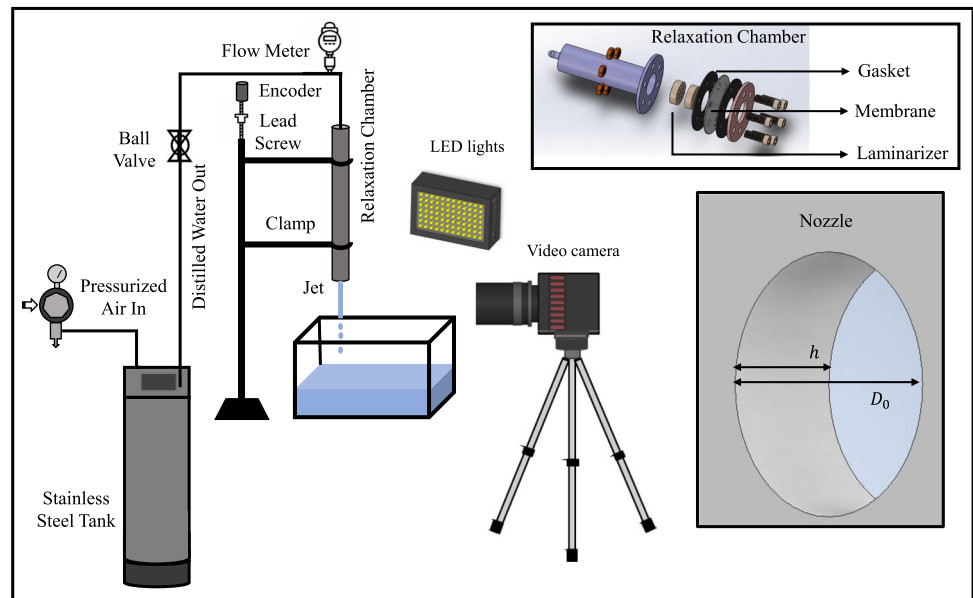
Silicon rubber membranes from which nozzles are cut and jets issue are sourced from McMaster-Carr and are

named by their shore A hardness assigned by the manufacturer. Shore A hardness for each material, excluding beryllium-copper (BeCu), is listed in the top row of Table 1. Assigning a single modulus to elastomers is not straightforward, as modulus is most often strain-dependent. However, we may approximate the modulus of each material using a the following relation [47],  $\log_{10} E = 0.0235S - 0.6403$ , where  $S = 70, 65, 35, 20$  is the shore A hardness. In addition to the modulus of each material, thickness  $h$  governs the ability of a material to deform. We determine the product of modulus and thickness, which has units of surface tension, to be the most appropriate metric to compare the deformability of our membranes. We report pertinent material properties in Table 1. Nozzles are generated in membranes with a circular punch, 500  $\mu\text{m}$  in diameter. In the case of the BeCu nozzle, a 1-mm punch is used. Initial nozzle diameter  $D_0$  (Table 1) is measured with a Keyence VHX-7000 digital microscope; nozzle diameter does not necessarily match punch diameter for reasons unknown.

Our jetting experiment is depicted in Fig. 2. A pressurized liquid reservoir, a ball-lock soda keg familiar to homebrewers, provides tap water to the relaxation chamber by way of a valve to control flow rate and a Micro-Flo FS1-201-6V digital paddlewheel flow meter. Water delivery with a pressurized vessel avoids in-line pressure pulses associated with pumps that affect jet breakup. The relaxation chamber is affixed to a linear stage that is mounted to a  $4' \times 10'$  Coherent optical table. The table is vibration-isolated by pneumatic legs. The liquid reservoir is also rests on the optical table. The linear stage is fitted with a Yumo E6A2-CW3C quadrature rotary encoder that records displacement via an Arduino Mega 2560 at a resolution of 0.025 mm, allowing precise quantification of breakup length. The relaxation chamber is constructed of 1" PVC, with internal acrylic laminarizers to straighten flow. The purpose of the 1-ft long relaxation chamber is to remove

**Table 1** Experimental material thickness  $h$ , estimated modulus  $E$ , functional stiffness  $Eh$ , and nominal nozzle diameter  $D_0$ . Materials are lists in order of decreasing functional stiffness

Material	BeCu	70A	65A	35A	35A	20A
$h$ ( $\mu\text{m}$ )	254	794	508	508	254	254
$E$ (MPa)	131,000	10.1	7.7	1.5	1.5	0.7
$Eh$ (kN/m)	33,275	8.02	3.92	0.77	0.39	0.17
$D_0$ ( $\mu\text{m}$ )	961	344	440, 490	495	540	450
Re	1840–21,600	3510–7390	3630–7490	2630–6210	2450–5370	870–3020
We	24–3261	344–2298	456–2503	173–1717	95–800	155–527
We <sub>G</sub>	0.03–3.91	0.41–2.76	0.55–3.00	0.21–2.06	0.11–0.96	0.19–0.63
$R^2$ , Eq. (4)	0.8288	0.9212	0.9020	0.8537	0.3411	0.6485

**Fig. 2** Experimental setup of jet stability through deformable nozzles. Insets show the assembly of the relaxation chamber and nozzle dimensions

the eddies generated as the flow expands from a narrow tube to a larger diameter membrane thereby delivering laminar flow to the nozzle. Nozzle membranes are sandwiched between an acrylic plate and galvanized iron flange at the end of the relaxation chamber. The flange has an inner diameter of 2.4 cm.

Our system is allowed to reach equilibrium after a new flow rate is chosen and before a video is captured. Jets issue vertically downward into a bucket. A Photron Nova S6 records jet breakup for 0.25 s at 8000 fps, and is fitted with a Nikon Micro-NIKKOR 55mm f/2.8 lens. The linear stage is adjusted such that the portion of the jet undergoing breakup appears in frame. Jets are backlit by custom-built LED lights such that jets appear black on a light background. High-speed videos are binarized frame-by-frame in MATLAB such that drops appear white against a black background. Doing so allows for the quantification of jet diameter and the pixel location of breaks in the jet, correlated to a physical scale.

### 3 Nozzle dilation

Static pressure behind our soft, elastic membranes (Fig. 2) beginning with 70A, results in stretching and deformation of the membrane. Radial strain of a membrane is much like the expansion of a balloon. Membranes stretch locally at the nozzle, limiting the jet velocities we can achieve with increasing flow rate. Nozzles expand more than  $2\times$  their initial diameter  $D_0$ . We estimate nozzle diameter at a fixed flow rate by measuring the diameter for a smooth, unbroken portion of the jet near the nozzle. We plot nozzle dilation  $\check{D} = D/D_0$  versus Reynolds number  $\text{Re} = \rho V_0 D/\mu$  in Fig. 3, where  $\mu = 0.89$  cP is the viscosity of water. It is difficult mathematically to predict how  $\check{D}$  will scale with Re, but our observations indicate that a useful approximation is  $\check{D} \sim \text{Re}$ , an approximation used for convenience such that we may compare dilation of the various membranes. We plot all such linear fits our dilation data in bottom-right panel of Fig. 3. Generally, softer membranes experience greater dilation, as expected, and are prone to failure at higher flow rates. The number of data

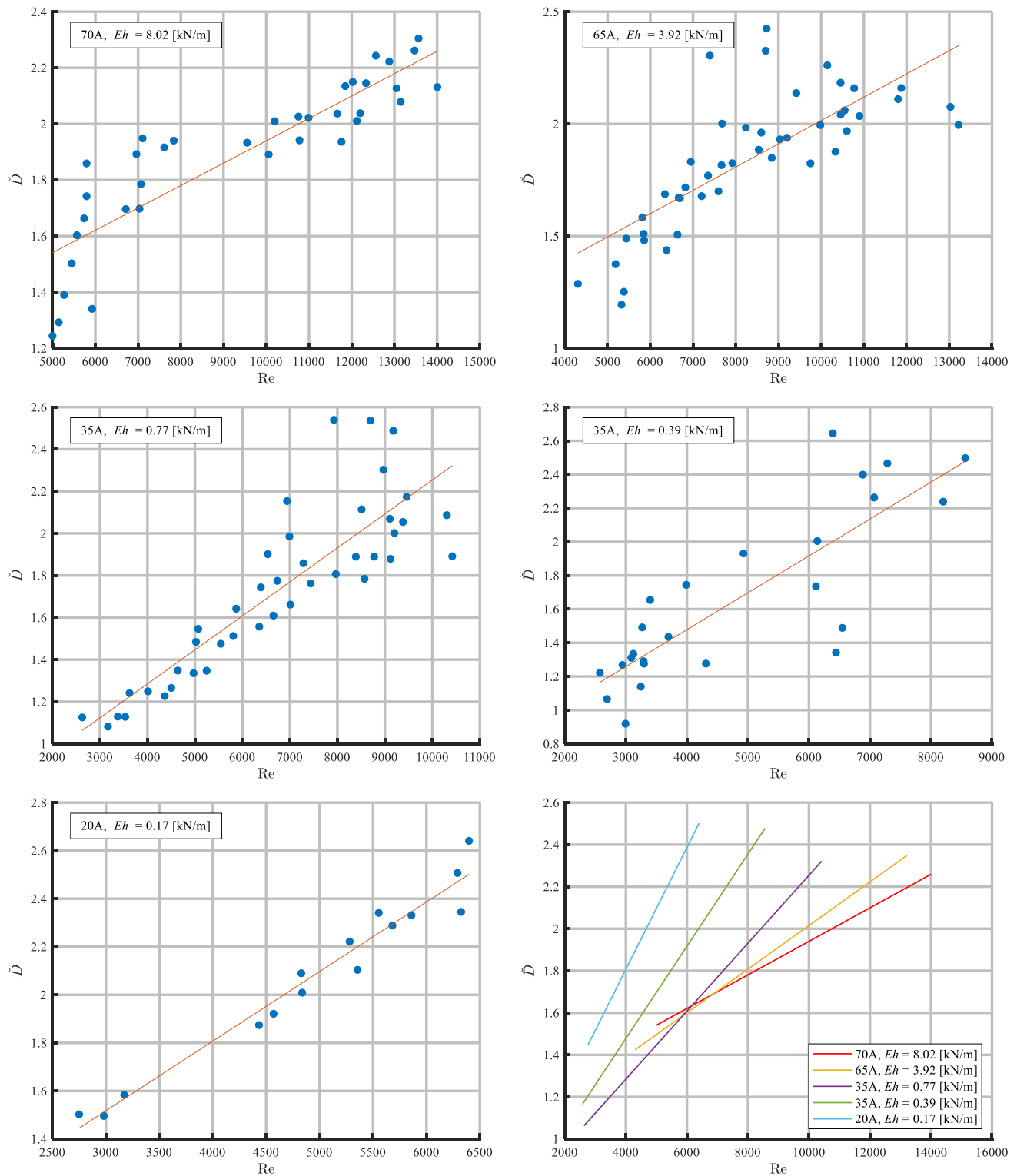


**Fig. 3** Nozzle dilation  $\dot{D}$  versus Reynolds number for experimental materials

points for the 20A material in Fig. 3 is limited because this material is exceedingly soft and delicate. We experience significant difficulties in producing more than one clean circular 20A nozzle with diameter comparable to other nozzles. The softer the material, the more it is pulled anisotropically during punching. The plotted data is from our ‘cleanest’ 20A nozzle with diameter closest to our target 500- $\mu\text{m}$  diameter. At  $\text{Re} \gtrsim 6500$ , the 20A material bursts. Dilution of a 20A nozzle over a range of flow rates is shown in Movie S1.

## 4 Scaling considerations for dilating nozzles

With knowledge that an increase in flow rate in our system does not proportionally increase exit velocity, due to nozzle dilation, we proceed with adapting conventional stability theory to our unique jets. Recent efforts using linear temporal theory for short nozzles [34] form the foundation of our stability analysis due to simplicity and ease of use. For rigid nozzles, breakup length  $Z$  in the Rayleigh and first wind-induced regimes is functionally proportional to velocity and increases with an increasing nozzle diameter. Such a relation is typically written [4, 5, 34]

$$Z/D = \ln(a/\zeta_0)[1 + 3\text{Oh}]\text{We}^{1/2}. \quad (1)$$

The Ohnesorge number  $\text{Oh} = \mu(\rho\sigma D)^{-1/2}$ ,  $a$  is jet radius, and  $\zeta_0$  is the initial dominant disturbance amplitude at the nozzle. It is traditionally assumed that  $\ln(a/\zeta_0)$  is constant [4, 5, 34]. We do the same here to assess the validity of this assumption with our nozzles, though we acknowledge that jet radius changes in our experiments and the nature of  $\zeta_0$  may well be non-constant as nozzles expand with increased flow rate. For our jets  $3\text{Oh} = O(0.01 - 0.1)$  and thus we neglect the second term of Eq. (1), and write the simplification as

$$Z/D \approx \ln(a/\zeta_0)\text{We}^{1/2}, \quad (2)$$

where  $\ln(a/\zeta_0)$  is a constant.

The use of Eq. (2) to predict breakup requires knowledge of both jet velocity exit  $V_0$  and nozzle diameter  $D$ . Furthermore, Eq. (2) by way of Eq. (1) was developed for constant  $D$ . In our jets, nozzle dilation modulates  $V_0$ , and without a high-speed camera,  $V_0$  is difficult to measure. Thus, a more convenient expression for breakup could be written with flow rate  $Q = \pi D^2 V_0/4$ , which is read directly from a flow meter,

$$Z/D \approx 4 \ln(a/\zeta_0)(\rho/D^3\sigma)^{1/2}Q/\pi. \quad (3)$$

By keeping liquid properties consistent in experiments, we may drop all constants in Eq. (2), or equivalently Eq. (3), to form a more concise relation that includes undeformed nozzle diameter  $D_0$ ,

$$Z/D_0 \sim \text{We}^{1/2}\check{D}. \quad (4)$$

From Eq. (4), we generally expect  $Z$  to increase with dilating nozzles and faster jets.

## 5 Jet stability

Jet stability through soft membranes should be considered in light of jets through a nozzle of a comparable, non-dilating shape. We begin by considering jets through a comparatively rigid beryllium-copper (BeCu) nozzle to establish a baseline of jet behavior through a planar nozzle. The stability curve for BeCu is shown at the top left of Fig. 4. In general, jets from planar nozzles are less stable than those which have a flow contraction before the exit [34], a fact which is unsurprising; liquids experience inherent flow disruption when rounding a sharp corner. Our nozzles are likely subject to *vena contracta*, a functional contraction of the nozzle at the entrance arising from flow separation [48]. If so, this initial disturbance of the jet is a contributor to the variance in breakup length we see with all our nozzles. The rigid, short but tapered nozzles of Etzold et al. (2018) produce non-dimensional breakup distances  $\approx 3\times$  greater than our BeCu sheet at comparable velocities. The breakup curve we report here is also noisy, or in other words, an increase in flow rate does not always produce the expected increase in breakup length.

Breakup length in our jets is not constant, oscillating by more than 5 jet diameters in some cases. For every video frame at 1/8000 s intervals we capture the length of unbroken liquid. Representative breakup length data for a single trial are shown in Fig. 5a, and the values of  $Z$  we report in Fig. 4 are the time average for 2000 frames. During this time, more than 700 droplets will exit the frame. Longer films may well produce differing breakup values, but this is as yet unknown. An FFT of the temporal breakup length signal of Fig. 5a, shown in Fig. 5b, demonstrates the presence of low frequency noise within the breakup signal, but periodicity is not discernible. For an ideal jet of constant breakup length, 700 droplets exiting in 0.25 s would equate a pinchoff frequency of 2.8 kHz and one would expect a spike at this frequency in an FFT. However, the frequency of drops passing a downstream point is not equal to, either instantaneously or time-averaged, the pinchoff frequency from the primary column. Short ligaments on occasion break into multiple drops. Discrete drops may overcome downstream counterparts and coalesce. The reader can infer such behaviors in the photographs of Fig. 1 and Movies S2–S4.

We fit Eq. (4) to the breakup data in Fig. 4 for all materials. For the four stiffest nozzles, Eq. (4) does a reasonable job of characterizing the breakup trend, with  $R^2$  values ranging from 0.83 to 0.92. The two softest nozzle display breakup trends which are more sporadic, and may be a result of the extreme strain these materials undergo at larger values of  $\text{We}^{1/2}\check{D}$ . Softer materials too may be more prone to vibrate under external forcing despite our best efforts to generate an isolated

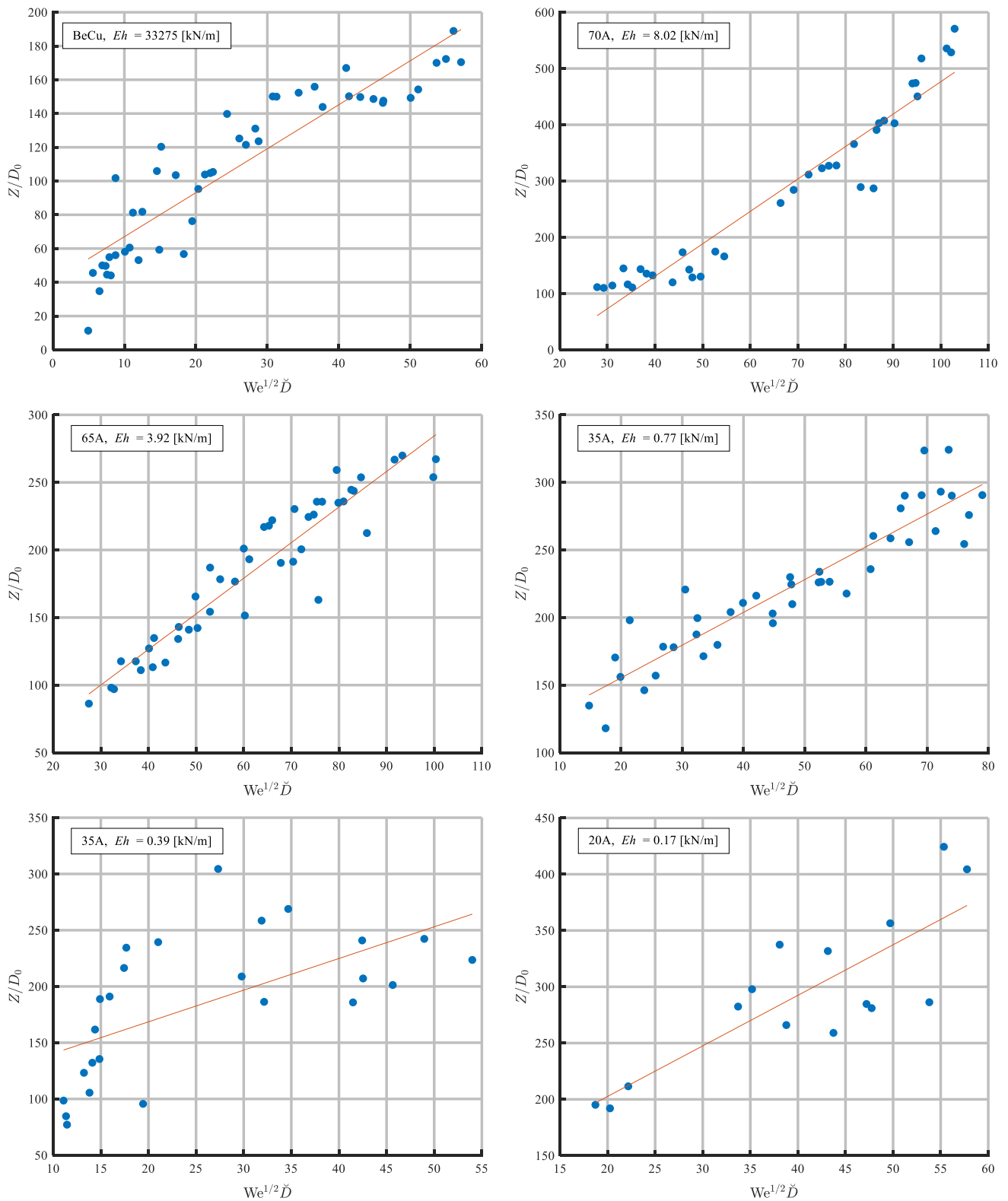


**Fig. 4** Stability curves for experimental materials in order of decreasing stiffness from left to right, top to bottom. Red lines correspond to the scaling relation predicted by Eq. (4)



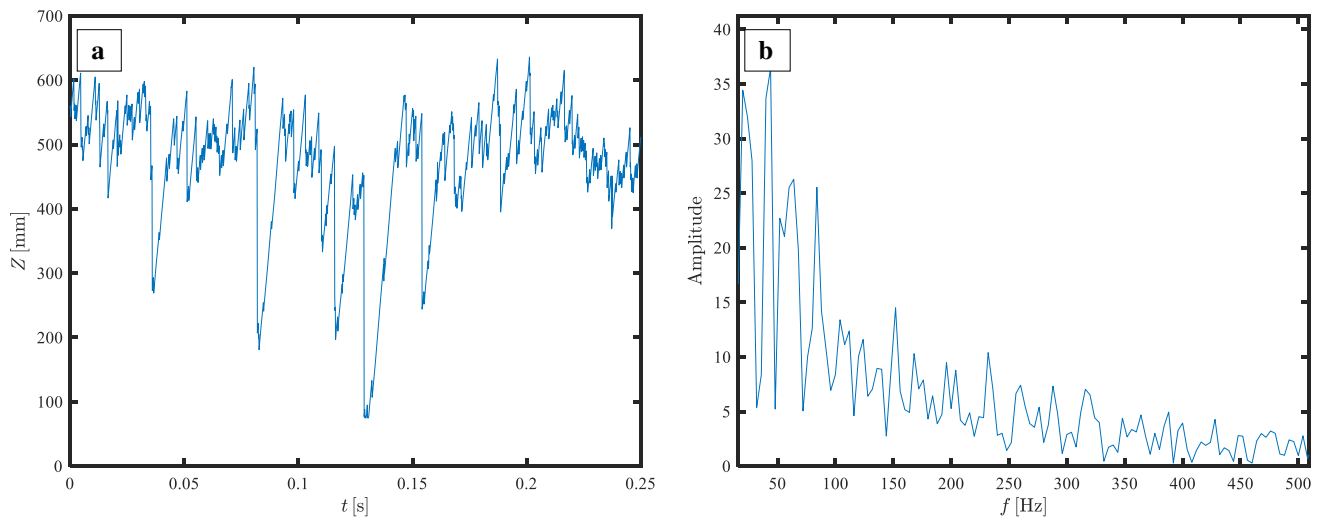


**Fig. 5** **a** Temporal breakup length for 35A [ $Eh = 0.77$  (kN/m)]. **b** FFT of data shown in **a**

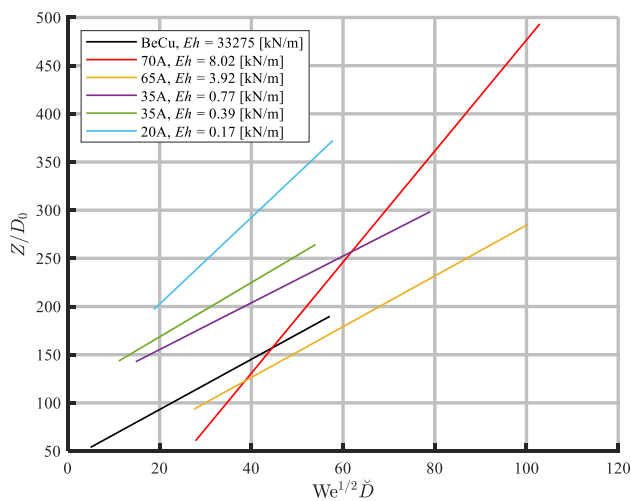


**Fig. 6** Stability curve linear fits based on the scaling in Eq. (4) for all experimental materials

system, or vibrate due to stochastic instabilities in the nozzle flow. A comparison of Eq. (4) fits for all materials is shown in Fig. 6, where the length of curves demonstrate the range of  $We^{1/2}\ddot{D}$  we are able to generate for each material. Membrane rupture limits the upper end of the softest materials and limitations in system flow rate is the constraint for materials which do not fail. In their operational range, the three softest materials produce the most stable jets for a fixed  $We^{1/2}\ddot{D}$ .

The anomalous slope of the 70A line in Fig. 6 may be due to their relative thickness,  $3\times$  that of the softest membranes, and such that  $h/D_0 = 2.3$ . The scatter of all materials in Fig. 4 hints at higher order complexities governing flow from these nozzles than breakup length alone can characterize. While these nozzles are short, their  $Re$  values indicate there may be turbulence present at the mouth of the nozzle. At a minimum, the transition from the liquid bulk to the nozzle flow is not

smooth. The length- and timescale nature of such turbulent fluctuation, how a disturbance is carried downstream, and how a compliant nozzle may respond to the turbulence is beyond the scope of this study.

## 6 Discussion and conclusions

As witnessed in our results, elasticity plays a significant role in both the jet velocity at various flow rates and the stability of jets. An untested method for modulating the effective elasticity of nozzles, and an area for future investigators, is changing the diameter of the membrane clamp. Adjusting clamp diameter is analogous to creating drumheads of differing size with the same tension; a larger drumhead vibrates at a lower frequency and greater amplitude. In our jets, a larger membrane area will permit more global deformation at an equivalent static pressure, and a corresponding change in nozzle shape. We cannot speculate on how stability curves will change with membrane area, but imagine jet stability may be modulated by both a new nozzle shape and vibration character of a larger ‘drumhead.’

A closer look at the strain field on the membranes with more advanced techniques such as digital speckle patterning [49] is likely to reveal more about what drives breakup length. Our unstrained membranes are functionally two-dimensional but become highly three-dimensional as static pressure in the relaxation chamber builds. As they strain, these elastomers exhibit a range of moduli [47], perhaps even a range of moduli over the area of the membrane itself. Thus, stretching governs the ability of a membrane to vibrate against the liquid globally and locally at the nozzle. Strain may not be uniform or asymmetric, particularly for nozzles which are not perfectly concentric to their clamp and those not perfectly circular. Future investigations should aim to connect strain fields and membrane vibration to the signal of breakup (Fig. 5a).

Despite the coupled behavior of membrane vibration, strain, and jet breakup, our work blazes a trail for a new method of targeted breakup characteristics. Customized stress–strain characteristics may be able to passively provide a desired diameter- and breakup-to-flow rate relationship. By tuning the vibratory characteristics of a membrane, it is possible to decrease jet stability with an increase in jet velocity for velocities that would otherwise fall within the Rayleigh breakup regime. In contrast, an elastic membrane's engineered damping may permit the suppression of external and upstream vibrations that seek to reduce jet stability. Materials and composite nozzles with high internal damping may dissipate vibration in part. Future work is aimed at creating pressure pulses upstream of the nozzle and monitoring how elastic nozzles reduce the influence of such disturbances on jet breakup.

As we consider the variables which emerge as one considers an engineered nozzle for controlling breakup in a manner similar to the presented here, the sheer number of variables begins to get grisly. Fluid variables consist of density, viscosity, surface tension, and velocity. Nozzle properties include diameter, thickness, elasticity. Further engineering the system with damping and/or induced vibration may add a number more. Thus, a jetting system as described is an excellent candidate for study by machine learning, in which a significant number of input variables can be used to predict an output variable, in this case, breakup length. Similar studies mating experimental results with machine learning include ejecting drops from driven cantilevers [50, 51] and drop impact onto a cantilevered fiber [52].

## 7 Data access

Raw experimental videos and data are publicly available in perpetuity via OneDrive. Interested parties should contact the corresponding author for access.

The online version contains supplementary material available at <https://doi.org/10.1140/epjs/s11734-022-00656-w>.

**Acknowledgements** We would like to thank the National Science Foundation (CBET-1941341) for support.

## References

1. G. Bidone, Expériences sur la forme et sur la direction des veines et des courans d'eau lancés par diverses ouvertures. Par Georges Bidone. De l'Imprimerie royale (1829)
2. F. Savart, Memoire sur la constitution des veines liquides lancees par des orifices circulaires en mince paroi. *Anal. Chem.* **53**, 337–386 (1833)
3. G. Amini, Y. Lv, A. Dolatabadi, M. Ihme, Instability of elliptic liquid jets: temporal linear stability theory and experimental analysis. *Phys. Fluids* **26**, 114105 (2014)
4. N. Ashgriz, A. Yarin, Capillary instability of free liquid jets. In *Handbook of Atomization and Sprays*, pp. 3–53. Springer (2011)
5. J. Eggers, E. Villermaux, Physics of liquid jets. *Rep. Prog. Phys.* **71**, 036601 (2008)
6. W. Sirignano, C. Mehring, Review of theory of distortion and disintegration of liquid streams. *Prog. Energy Combust. Sci.* **26**, 609–655 (2000)
7. V. Entov, A. Yarin, The dynamics of thin liquid jets in air. *J. Fluid Mech.* **140**, 91–111 (1984)
8. V. Entov, A. Yarin, Dynamical equations for a liquid jet. *Fluid Dyn.* **15**, 644–649 (1980)
9. N.M. Smith, H. Ebrahimi, R. Ghosh, A.K. Dickerson, High-speed microjets issue from bursting oil gland reservoirs of citrus fruit. *Proc. Natl. Acad. Sci. ISSN* 0027-8424 (<https://doi.org/10.1073/pnas.1720809115>) (2018)
10. D. Jarrahbashi, W.A. Sirignano, Acceleration effects on instability of high-pressure fuel jets. In *Proceedings of the Twelfth International Conference on Liquid Atomization and Spray Systems (ICLASS)* (2012)
11. S. Mitragotri, Current status and future prospects of needle-free liquid jet injectors. *Nat. Rev. Drug Discov.* **5**, 543–548 (2006)
12. D.H. Reneker, A.L. Yarin, H. Fong, S. Kooimbhongse, Bending instability of electrically charged liquid jets of polymer solutions in electrospinning. *J. Appl. Phys.* **87**, 4531–4547 (2000)
13. V. Menezes, S. Kumar, K. Takayama, Shock wave driven liquid microjets for drug delivery. *Phys. Fluids* **106** (2009)
14. Y. Tagawa, N. Oudalov, A. El Ghalbzouri, C. Sun, D. Lohse, Needle-free injection into skin and soft matter with highly focused microjets. *Lab Chip* **13**, 1357–1363 (2013)
15. E.P. Furlani, B.G. Price, G. Hawkins, A.G. Lopez, Thermally induced marangoni instability of liquid microjets with application to continuous inkjet printing. In *Proceedings of NSTI Nanotechnology Conference* (2006)
16. J.C. Carter, R.M. Alvis, S.B. Brown, K.C. Langry, T.S. Wilson, M.T. McBride, M. Myrick, W.R. Cox, M.E. Grove, B.W. Colston, Fabricating optical fiber imaging sensors using inkjet printing technology: a ph sensor proof-of-concept. *Biosens. Bioelectron.* **21**, 1359–1364 (2006)
17. D. MacFarlane, V. Narayan, J. Tatum, W. Cox, T. Chen, D. Hayes, Microjet fabrication of microlens arrays. *IEEE Photonics Technol. Lett.* **6**, 1112–1114 (1994)
18. A. Guha, R.M. Barron, R. Balachandar, An experimental and numerical study of water jet cleaning process. *J. Mater. Process. Technol.* **211**, 610–618 (2011)
19. M. Krsmanovic, D. Biswas, H. Ali, A. Kumar, R. Ghosh, A.K. Dickerson, Hydrodynamics and surface properties influence biofilm proliferation. *Adv. Colloid Interface Sci.* **288**, 102336 (2021)
20. Y.-P. Zhang, S.-H. Lee, K.R. Reddy, A.I. Gopalan, K.-P. Lee, Synthesis and characterization of core-shell SiO<sub>2</sub> nanoparticles/poly (3-aminophenylboronic acid) composites. *J. Appl. Polym. Sci.* **104**, 2743–2750 (2007)
21. L. Rayleigh, On the instability of jets. *Proc. Lond. Math. Soc.* **1**, 4–13 (1878)
22. A. Gañán-Calvo, A. Barrero, A novel pneumatic technique to generate steady capillary microjets. *J. Aerosol*



- Sci. **30**, 117–125 (1999). [https://doi.org/10.1016/S0021-8502\(98\)00029-9](https://doi.org/10.1016/S0021-8502(98)00029-9). (ISSN 0021-8502)
23. C.M. Varga, J.C. Lasheras, E.J. Hopfinger, Initial breakup of a small-diameter liquid jet by a high-speed gas stream. *J. Fluid Mech.* **497**, 405–434 (2003)
  24. K. Rajesh, R. Sakthikumar, D. Sivakumar, Interfacial oscillation of liquid jets discharging from non-circular orifices. *Int. J. Multiphase Flow* **87**, 1–8 (2016)
  25. A.H. Lefebvre, V.G. McDonell, *Atomization and Sprays* (CRC Press, Boca Raton, 2017)
  26. Y. Song, D. Hwang, K. Ahn. Effect of orifice geometry on spray characteristics of liquid jet in cross flow. In 55th AIAA Aerospace Sciences Meeting, p. 1961 (2017)
  27. J. Blaisot, S. Adeline, Instabilities on a free falling jet under an internal flow breakup mode regime. *Int. J. Multiphase Flow* **29**, 629–653 (2003)
  28. G. Amini, A. Dolatabadi, Capillary instability of elliptic liquid jets. *Phys. Fluids* **23**, 084109 (2011)
  29. G. Amini, A. Dolatabadi, Axis-switching and breakup of low-speed elliptic liquid jets. *Int. J. Multiphase Flow* **42**, 96–103 (2012)
  30. A. Kalaaji, B. Lopez, P. Attane, A. Soucemarianadin, Breakup length of forced liquid jets. *Phys. Fluids* **15**, 2469–2479 (2003)
  31. S. Lin, R. Reitz, Drop and spray formation from a liquid jet. *Annu. Rev. Fluid Mech.* **30**, 85–105 (1998)
  32. Wv. Ohnesorge, Formation of drops by nozzles and the breakup of liquid jets. *Z. Angew. Math. Mech.* **16**, 355–358 (1936)
  33. W. Ranz, On Sprays and Spraying (Pennsylvania State University Bulletin, Department of Engineering Research, 1956)
  34. M. Etzold, A. Deswal, L. Chen, F. Durst, Break-up length of liquid jets produced by short nozzles. *Int. J. Multiphase Flow* **99**, 397–407 (2018)
  35. A.M. Sterling, C. Sleicher, The instability of capillary jets. *J. Fluid Mech.* **68**, 477–495 (1975)
  36. N. Ashgriz (ed.), *Handbook of Atomization and Sprays: Theory and Applications*. Springer. ISBN 1441972641 (2011)
  37. L. Rayleigh, On the capillary phenomena of jets. *Proc. R. Soc. Lond.* **29**, 71–97 (1879)
  38. C. Weber, Zum zerfall eines flüssigkeitsstrahles. *J. Appl. Math. Mech.* **11**, 136–154 (1931)
  39. J. Gordillo, M. Pérez-Saborid, Aerodynamic effects in the break-up of liquid jets: on the first wind-induced break-up regime. *J. Fluid Mech.* **541**, 1–20 (2005)
  40. N. Ashgriz, F. Mashayek, Temporal analysis of capillary jet breakup. *J. Fluid Mech.* **291**, 163–190 (1995)
  41. R. REITZ, Modeling atomization processes in high-pressure vaporizing sprays. *Atomisation Spray Technol.* **3**, 309–337 (1987)
  42. R. Reitz, F. Bracco, Mechanism of atomization of a liquid jet. *Phys. Fluids* **25**, 1730–1742 (1982)
  43. D. Boggy, Breakup of a liquid jet: third perturbation Cosserat solution. *Phys. Fluids* **22**, 224–230 (1979)
  44. D. Boggy, Break-up of a liquid jet: second perturbation solution for one-dimensional Cosserat theory. *IBM J. Res. Dev.* **23**, 87–92 (1979)
  45. D. Boggy, Wave propagation and instability in a circular semi-infinite liquid jet harmonically forced at the nozzle. *J. Appl. Mech.* **45**, 469–474 (1978)
  46. D. Boggy, Use of one-dimensional cosserat theory to study instability in a viscous liquid jet. *Phys. Fluids* **21**, 190–197 (1978)
  47. K. Larson, *Can you estimate modulus from durometer hardness for silicones?* (Technical report, Dow Corning Coroporation, 2016)
  48. M.P. Wilson Jr., R.G. Teyssandier, The Paradox of the Vena Contracta. *J. Fluids Eng.* **97**, 366–371 (1975). <https://doi.org/10.1115/1.3447316>. (ISSN 0098-2202)
  49. D. Amodio, G. Broggiato, F. Campana, G. Newaz, Digital speckle correlation for strain measurement by image analysis. *Exp. Mech.* **43**, 396–402 (2003)
  50. M.E. Alam, D. Wu, A.K. Dickerson, Predictive modelling of drop ejection from damped, dampened wings by machine learning. *Proc. R. Soc. A* **476**, 20200467 (2020)
  51. M.E. Alam, J.L. Kauffman, A.K. Dickerson, Drop ejection from vibrating damped, dampened wings. *Soft Matter* **16**, 1931–1940 (2020)
  52. P. Orkweha, A. Downing, A.P. Lebanoff, S. Zehtabian, S.S. Bacanli, D. Turgut, A.K. Dickerson, Ensemble machine learning predicts displacement of cantilevered fibers impacted by falling drops. *J. Fluids Struct.* **102**, 103253 (2021)

Springer Nature or its licensor holds exclusive rights to this article under a publishing agreement with the author(s) or other rightsholder(s); author self-archiving of the accepted manuscript version of this article is solely governed by the terms of such publishing agreement and applicable law.